Experimental research on application of Hartmann micro-lens array in coherent beam combination of two-dimensional laser array

Xiaohua Wang (王晓华)[1,2,3*], Qiang Fu (付 强)[1,2,3], Linhai Huang (黄林海)[1,2], Feng Shen (沈 锋)[1,2], and Changhui Rao (饶长辉)[1,2]

[1] *The Laboratory on Adaptive Optics, Institute of Optics and Electronics, Chinese Academy of Sciences, Chengdu 610209, China*

[2] *The Key Laboratory on Adaptive Optics, Chinese Academy of Sciences, Chengdu 610209, China*

[3] *Graduate University of Chinese Academy of Sciences, Beijing 100049, China*

[*] *Corresponding author: wxhua009@163.com*

Received November 9, 2011; accepted February 24, 2012; posted online April 20, 2012

We demonstrate experimentally the application of a phase error detection method in the coherent beam combination (CBC) of a laser array. The method is based on the Hartmann micro-lens array. Both the piston and tilt errors can be detected and corrected simultaneously by combining this method with adaptive optics-correcting technology. The far-field intensity pattern of the combined beam has high energy concentration and good beam quality. The power encircled in the main lobe of the far-field pattern is 41.3%, and the contrast of the pattern reaches 81.8%. Experimental results show the great potential of the Hartmann phasing method for use in the CBC of a large number of laser beams.

OCIS codes: 140.3298, 110.1080, 120.5050.

doi: 10.3788/COL201210.081402.

The coherent beam combination (CBC) of single mode lasers is a reliable method to acquire high-power or high-brightness beams with good beam qualities. Compared with the single high-power lasers, combining several low-power laser beams coherently has advantages in terms of thermal loading distribution and reduction of the diffraction angle. The coherent combining approaches can be classified mainly into active phasing[1−5] and passive phasing[6−9]. The active phasing is mostly based on the master oscillator power amplifier (MOPA) configuration[2−4], in most of which the fiber phase modulators are inserted before the fiber amplifiers to compensate for the piston aberrations. In some other configurations, the adaptive optics (AO) technologies, such as active segmented mirror (ASM)[5,10] and adaptive photonics phase-locked elements (APPLE)[11], are employed to perform this task. In addition, the steering mirrors and deformable mirrors can be used to correct tip-tilt and higher-order aberrations, respectively[2]. Some of the active phasing methods, such as heterodyne[2,12] and zero-order interference (ZOI) detections, need an external reference beam, while others do not, such as Self-Synchronous and Self-Reference[3] and SPGD algorithm control[4,11]. Most of these techniques extract the phase errors from the signals coming from the photo-detectors with a pinhole. Another type of phasing method[13−16] is applied in phasing large segmented telescopes in order to detect the piston errors between two neighboring apertures or segmented mirrors. These methods measure the piston errors by processing the interference images of the two apertures. Some of these methods have been used to detect the piston errors in two-beam CBC[15,17]. For a multi-aperture case, the Hartmann sensor is first applied to phase the 36 primary mirror segments in Keck telescopes[16]. A simulation work[18] demonstrates the application of a Hartmann sensor in multi-beam CBC. In these applications, Hartmann sensors are employed to acquire the interference images of two neighboring apertures or beams. Apart from piston error detection, the Hartmann sensor can also perform tilt error detection simultaneously.

In this letter, we demonstrate experimentally the method of piston and tilt error detection using a Hartmann sensor in a three-beam CBC system based on adaptive optics. Three beams were created by a low-power plane wave passing through an aperture screen in order to demonstrate how the method works. The piston and tilt errors were then introduced by a heater and a signal generator, respectively.

The experimental three-beam CBC setup based on AO is shown in Fig. 1. A He-Ne laser source produced a line-polarized beam with a wavelength of 632.8 nm. The laser beam was expanded to a plane wave with 50-mm diameter by passing through an intensity adjuster, a 40× micro-objective lens (MOL), a pinhole with a diameter of 20 μm, and a collimator lens (lens1, f = 400 mm). An aperture screen cut the plane wave into 3 beams with 14-mm diameter and 16-mm center separation. The apertures were center aligned with the sub-mirrors of ASM used to correct the piston and tilt errors. The beams were first split by a beam splitter (BS1) into two parts: one part passed through the turbulence and was reflected by ASM; the other was reflected by a high reflective mirror (HRM). The first part was used for the CBC experiment, and the second was used to calibrate the micro-lens array (MLA). These two parts should not work simultaneously, i.e., when one is working, the other should be stopped. Another beam splitter (BS2) split the input beams into two parts: one part was for the sample system, and the beams were focused by lens4

(f = 220 mm) and recorded by a CCD camera with a 40× micro-objective lens; the other was for the Hartmann wavefront sensing system. By passing through a 1/8× beam-reducing system, which was combined by lens2 (f =440 mm) and lens3 (f = 55 mm), the beams were dissected into a number of small samples using the MLA (f = 300 mm), which then focused the light onto a high-speed CMOS camera. The ASM, lens2, lens3, and MLA were placed precisely to create a 4-f Fourier imaging system. The images recorded by the CMOS were then sent to the computer-based AO control platform, which extracted the piston and tilt errors and generated control signals for the ASM. A signal generator provided 3-Hz sinusoidal signals with 1-V amplitude used to introduce piston noises. Despite this weak signal, it provided piston noise over 2 π. The control signals, combined with the noise signals, were sent to the high voltage amplifier (HVA) to drive the ASM. The CMOS had a frame rate of nearly 560 fps at a resolution of 512 × 512 pixels, but the efficient frame rate was reduced to 330 fps because the computer used some time to calculate the control signals. Note that the slow disturbing signal was used to demonstrate how the CBC setup work can compensate dynamic piston noises, but not to present how fast the control bandwidth was.

The configuration and dimensions of the ASM are shown in Fig. 2(a). Each sub-mirror has three piezoceramic actuators, so it has three degrees of freedom: piston, tip, and tilt.

The arrangements of the input beams and the Hartmann sensor are shown in Fig. 2(b). The incident beams are reduced from a diameter of 14 to 1.75 mm. The shape of the micro-lens was designed to be orthohexagonal in order to allow more light to pass through it. The micro-lenses with numbers 1, 4, and 6 were center aligned with 3 input beams; these were used to measure the tilt errors of each incident beam. The ones with numbers 2, 3, and 5 were used to measure the piston errors between

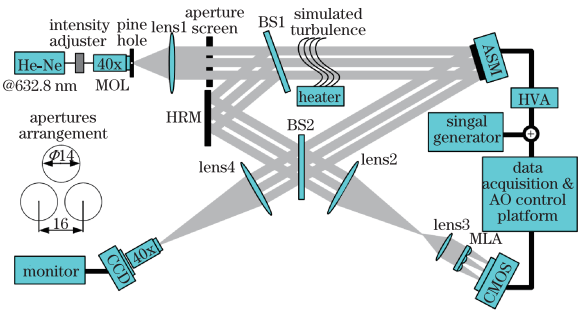

Fig. 1. Schematic of the experimental CBC setup.

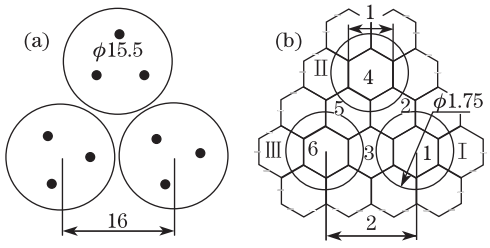

Fig. 2. (a) Configuration of ASM; (b) arrangements of reduced beams (circles) and MLA (orthohexagonals), and the dashed micro-lens are not in use (default unit: mm).

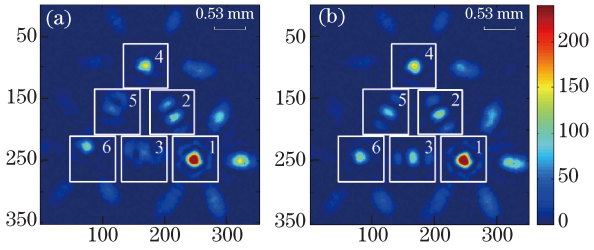

Fig. 3. Focal spots of light created by MLA (a) before and (b) after the correction of the phase errors. The spots enclosed in the numbered squares correspond to the micro-lens with the same number.

the corresponding two beams. Figures 3(a) and (b) show the focal spots of light created by the MLA before and after the correction of the phase errors (piston and tilt), respectively. The spots enclosed in the numbered squares correspond to the micro-lenses with the same number. Given that the third beam has big tilt errors, the patterns in segments 3 and 5 in Fig. 3(a) are blurred. In order to obtain clearer inference patterns, the tilt errors of the beams should be eliminated first.

The tilt error of each beam can be measured by the center-of-mass algorithm[19]. The piston detection method is similar to the technique used in[16]. The location of the peak intensity of the interference pattern changes with the piston error. Figure 4 shows that the peak location of the pattern of the third micro-lens varies with the piston error generated by ASM in the experiment. The peak shifts linearly with the piston error in the period of $-\lambda/2$ to $\lambda/2$. When the piston error equals $-\lambda/2$ or $\lambda/2$, the peak location jumps from the lower limit to the higher limit, because the peak intensity shifts from one side lobe to the other.

In the experiment, the piston and tilt controls are independent, and both adopt the traditional PID control algorithm. The experiment is divided into three phases. In the first phase, both the piston and tilt controls are off, and the system works in a free running mode. The long-exposure far-field intensity distributions are shown in Figs. 5(a) and (e), and as can be seen, the central intensity is quite low. In the second phase, the tilt control is on, but the piston control is still off. As the tilt errors are corrected, the beams are converged stably on the center than in free running. The pattern on the observing plane is blurred because of the piston errors. The central intensity is promoted by 1.8 times than in free running, and the long-exposure far-field intensity distributions are shown in Figs. 5(b) and (f). In the last phase, both the piston and tilt control are on. When the piston errors are eliminated, the pattern on the observing plane is similar to the diffraction-limited shape. The central intensity is nearly 4 times than the one in free running. The long-exposure far-field intensity distributions are shown in Fig. 5(c) and (g), and the theoretical far-field patterns are shown in Fig. 5(d) and (h). We adopted the fringe contrast to measure the beam quality of far-field pattern. It is defined as $(I_{\max} - I_{\min})/(I_{\max} + I_{\min})$, where $I_{\max}$ and $I_{\min}$ are the maximum intensity and the adjacent minimum of the intensity pattern respectively. The fringe contrast of the pattern in Fig. 5(c) is calculated to be 81.8%. The power encircled in the main lobe is 41.3% of the total power of the pattern, compared with

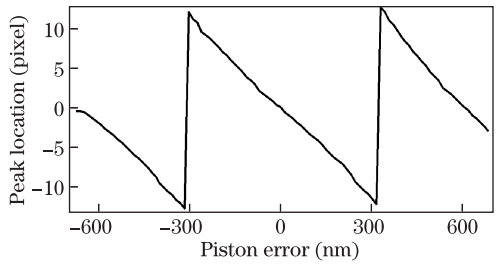

Fig. 4. Experimental results of the peak location shift varying with the piston error generated by the ASM ($\lambda g = 632.8$ nm).

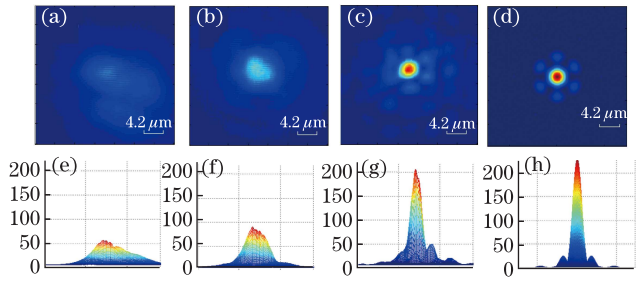

Fig. 5. Long-exposure far-field intensity distributions of the combined beams. (a) Both piston and tilt control are off, (b) only tilt control is on, (c) both piston and tilt control are on, (d) theoretical, and (e), (f), (g) and (h) are their intensity distributions along the x axis, respectively.

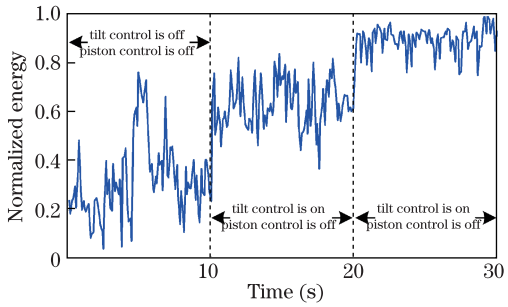

Fig. 6. Normalized energy encircled in the main lobe area of the far-field patterns in different phases.

the theoretical value of 57.8% in Fig. 5(d). The energy encircled in the area of the main lobe is calculated from the videos recorded by the CCD camera. The normalized curves in the whole experiment are shown in Fig. 6. The tilt correction eliminates the beam excursion, thus promoting energy concentration. Once the piston correction is added in, the energy is more concentrated in the main lobe area. The results agree with the long-exposure far-field patterns.

The advantage of this method is that it can measure the piston and tilt errors simultaneously and precisely. If the beam number is big enough, the piston phase may be tightly locked from beam to beam. There would be cumulative errors in piston detection, which would degrade the beam quality in the far-field. It is a problem that must be resolved while the method is applied in large laser array CBC. To increase the control bandwidth, CMOS with higher speed can be used and the image processing can be executed in high speed DSP modules.

In conclusion, we have demonstrated the application of the Hartmann sensor in measuring the phase errors (piston and tilt) in coherently combining a two-dimensional three-beam laser array. It can detect the piston and tilt errors simultaneously. With the help of correction system based on AO technology, the output of the CBC is steady with high energy concentration and good beam quality. The power encircled in the main lobe is 41.3% compared with the theoretical value of 57.8%. The central brightness is scaled to 4 times than in free running, whereas the contrast of the combined beam profile in closed loop is 81.8%. The experimental results present that the Hartmann phase-error detecting method works efficiently in CBC and has the potential for use in coherently combining a large laser array.

This work was supported by the Advanced Research Foundation for National Defense Science and Technology of China under Grant No. A06K024.

References

1. G. D. Goodno, C. P. Asman, J. Anderegg, S. Brosnan, E. C. Cheung, D. Hammons, H. Injeyan, H. Komine, W. H. Long, M. McClellan, S. J. McNaught, S. Redmond, R. Simpson, J. Sollee, M. Weber, S. B. Weiss, and M. Wickham, IEEE J. Sel. Top. Quantum Electron. **13,** 460 (2007).
2. G. D. Goodno, H. Komine, S. J. McNaught, S. B. Weiss, S. Redmond, W. Long, R. Simpson, E. C. Cheung, D. Howland, P. Epp, M. Weber, M. McClellan, J. Sollee, and H. Injeyan, Opt. Lett. **31,** 1247 (2006).
3. T. M. Shay, V. Benham, J. T. Baker, A. D. Sanchez, D. Pilkington, and C. A. Lu, IEEE J. Sel. Top. Quantum Electron. **13,** 480 (2007).
4. X. Li, X. Dong, H. Xiao, X. Wang, and X. Xu, Chin. Opt. Lett. **9,** 101401 (2011).
5. R. Yang, P. Yang, L. Dong, M. Ao, and B. Xu, Appl. Phys. B **99,** 19 (2010).
6. B. Wang, E. Mies, M. Minden, and A. Sanchez, Opt. Lett. **34,** 863 (2009).
7. M. Fridman, V. Eckhouse, N. Davidson, and A. A. Friesem, Opt. Lett. **32,** 790 (2007).
8. W. Wang, B. He, H. Zhang, Y. Xue, Z. Li, X. Liu, J. Zhou, and Q. Lou, Chin. Opt. Lett. **8,** 680 (2010).
9. J. Morel, A. Woodtli, and R. Dandliker, Opt. Lett. **18,** 1520 (1993).
10. Y. Zheng, X. Wang, L. Deng, F. Shen, and X. Li, Appl. Opt. **50,** 2239 (2011).
11. L. Liu, M. A. Vorontsov, E. Polnau, T. Weyrauch, and L. A. Beresnev, Proc. SPIE **6708,** 67080K (2007).
12. J. Anderegg, S. Brosnan, E. Cheung, P. Epp, D. Hammons, H. Komine, M. Weber, and M. Wickham, Proc. SPIE **6102,** 61020U (2007).
13. S. Esposito, E. Pinna, A. Puglisi, A. Tozzi, and P. Stefanini, Opt. Lett. **30,** 2572 (2005).
14. K. L. Baker, D. Homoelle, E. Utterback, and S. M. Jones, Opt. Express **17,** 19551 (2009).
15. S. C. West, Appl. Opt. **41,** 3781 (2002).
16. G. Chanan, M. Troy, F. Dekens, S. Michaels, J. Nelson, T. Mast, and D. Kirkman, Appl. Opt. **37,** 140 (1998).
17. P. Yang, R. Yang, F. Shen, X. Li, and W. Jiang, Opt. Commun. **282,** 1349 (2009).
18. P. Yang, R. Yang, L. Dong, X. Lei, and B. Xu, Appl. Phys. B **98,** 465 (2010).
19. D. R. Neal, W. J. Alford, and J. K. Gruetzner, Proc. SPIE **2870,** 72 (1996).